International Journal of Pharmaceutics 646 (2023) 123502

Contents lists available at ScienceDirect

International Journal of Pharmaceutics

journal homepage: www.elsevier.com/locate/ijpharm

Real-time *in vivo* monitoring of the antimicrobial action of combination therapies in the management of infected topical wounds

Guillermo Landa [a,b,c], Laura G. Miranda-Calderon [a,b], Alex Gomez [d,e], Marta Perez [e,f], Victor Sebastian [a,b,c,g], Manuel Arruebo [a,b,c,g,*], Isabelle Lamarche [h], Frederic Tewes [h,*], Silvia Irusta [a,b,c,g], Gracia Mendoza [c,g]

[a] *Instituto de Nanociencia y Materiales de Aragón (INMA), CSIC-Universidad de Zaragoza, 50009 Zaragoza, Spain*
[b] *Department of Chemical and Environmental Engineering. University of Zaragoza, Campus Río Ebro-Edificio I+D, C/ Poeta Mariano Esquillor S/N, 50018 Zaragoza, Spain*
[c] *Aragon Health Research Institute (IIS Aragon), 50009 Zaragoza, Spain*
[d] *Department of Animal Pathology, University of Zaragoza, 177 Miguel Servet Street, 50013 Zaragoza, Spain*
[e] *Instituto Universitario de Investigación Mixto Agroalimentario de Aragón (IA2), University of Zaragoza, 50013 Zaragoza, Spain*
[f] *Department of Anatomy, Embriology and Animal Genetics, University of Zaragoza, 177 Miguel Servet Street, 50013 Zaragoza, Spain*
[g] *Networking Research Center on Bioengineering, Biomaterials and Nanomedicine, CIBER-BBN, 28029 Madrid, Spain*
[h] *INSERM U1070 "Pharmacology of anti-infective agents", 1 rue Georges Bonnet, Pôle Biologie Santé, 86022 Poitiers, France*

ARTICLE INFO

Keywords:
Drug delivery
Wound dressing
Electrospinning
Chlorhexidine
Farnesol
Thymol

ABSTRACT

The increasing prevalence of non-healing infected wounds has become a serious concern in the clinical practice, being associated to population aging and to the rising prevalence of several chronic conditions such as diabetes. Herein, the evaluation of the bactericidal and antibiofilm effects of the natural antiseptic terpenes thymol and farnesol standing alone or in combination with the standard care antiseptic chlorhexidine was carried out both *in vitro* and *in vivo*. The *in vitro* combinatorial treatment of chlorhexidine associated with those terpenes against *Staphylococcus aureus* in its planktonic and sessile forms demonstrated a superior antibacterial activity than that of chlorhexidine alone. Real-time *in vivo* monitoring of infection progression and antimicrobial treatment outcomes were evaluated using the bioluminescent *S. aureus* strain Xen36. *In vivo* studies on infected wound splinting murine models corroborated the superior bactericidal effects of the combinatorial treatments here proposed. Moreover, the encapsulation of thymol in electrospun Eudragit® S100 (i.e., a synthetic anionic copolymer of methacrylic acid and ethyl acrylate)-based wound dressings was also carried out in order to design efficient antimicrobial wound dressings.

1. Introduction

Acute cutaneous damage (mechanical trauma, surgery-associated, burns, etc.) is a common health problem that can have serious systemic consequences when the skin physiology is not rapidly restored. Therefore, wound healing is a physiological requirement to guarantee the maintenance of human health and well-being (Krizanova et al., 2022). The healing process begins immediately after wounding and continues for a variable period of time depending on the severity of the wound and its characteristics (i.e., acute, chronic). It is necessary to use efficient treatments to accelerate the healing process at all its stages to quickly restore the structure and function of the skin tissue (Mirhaj et al., 2022). These stages include the initial acute inflammatory response with blood coagulation and hemostasis, followed by cell proliferation, migration, regeneration, and finally, connective tissue remodeling. In healthy skin, the acidic keratin sebum and eccrine secretions maintain its pH slightly acidic (around 5.5), but, when a wound occurs, this pH shifts to an alkaline range which varies between 7 and 10 due to the exposure of the underlying tissues. The increase in pH could lead to complications such as the growth of commensal or exogenous bacteria on the wound bed, acceleration of transepidermal water loss, and change in the skin microbiome (Ullah et al., 2021).

The presence of bacterial biofilm impairs and delays the physiological wound healing process because it constitutes a barrier not only

* Corresponding authors at: Networking Research Center on Bioengineering, Biomaterials and Nanomedicine, CIBER-BBN, 28029 Madrid, Spain (M. Arruebo).
E-mail addresses: arruebom@unizar.es (M. Arruebo), frederic.tewes@univ-poitiers.fr (F. Tewes).

https://doi.org/10.1016/j.ijpharm.2023.123502
Received 25 August 2023; Received in revised form 27 September 2023; Accepted 9 October 2023
Available online 10 October 2023

against exogenous antimicrobial treatments but also against the host immune response (Wei et al., 2019). Bacterial biofilm is formed by an extracellular polymeric substance, composed of polysaccharides, proteins, DNA, and lipids, which protects bacteria against the response of the hosts immune system and against antimicrobial treatments (Phillips et al., 2015).

Staphylococcus aureus is a prevalent commensal pathogen commonly present on infected wounds. It has the ability to rapidly form biofilms on the wound bed and also can persist intracellularly forming the as called, small colony variants, which are characteristic for their high virulence (Zheng et al., 2021). The use of antibacterial wound dressings is intended to reduce the bacterial burden and prevent biofilm formation, thus shortening the healing period after wounding (Jian et al., 2023, 2020; Li et al., 2022).

Previous investigations have demonstrated the potential use of multifunctional biomaterials for staged wound healing (Luo et al., 2022) or on-demand wound repair (Yang et al., 2023). In fact, polymeric nano and microfibrous structures are the most widely applied wound dressings for skin repair and regeneration owed to their highly porous structure and large surface area which favor gas exchange and proper wound drainage (Huanbutta et al., 2019). Among current techniques for the fabrication of nanofibrous structures, electrospinning allows the fabrication of multifunctional dressings with enhanced mechanical, chemical, and physical properties. This method allows the encapsulation within the electrospun fibers of antimicrobial drugs with the consequent protection and controlled release ability (Parham et al., 2022). Both hydrophobic and hydrophilic drugs can be encapsulated into electrospun fibers and drug-loaded nanofibrous dressings and can be applied topically on the wound bed or as a postoperative prophylactic dressing to prevent microbial proliferation (Zamani et al., 2013).

Due to the increased antibiotic resistance, the use of natural plant-derived compounds is being investigated for their therapeutic potential, as they show multiple mechanisms of antimicrobial action and the chances to develop phenotypic adaptations to several targets are reduced, contrary to antibiotics that usually have only one target (García-Salinas et al., 2020a). Electrospun fibers loaded with active substances derived from essential oils such as thymol (THY) and carvacrol (Gámez et al., 2020, 2019; Gámez-Herrera et al., 2020; Garcia-Salinas et al., 2020) have been previously developed. We have previously shown that THY-loaded electrospun dressings based on polycaprolactone (PCL) are able to eliminate an experimental topical infection *in vivo* producing similar outcomes than the conventional strong antiseptic chlorhexidine but with reduced tissue toxicity (García-Salinas et al., 2020b). Farnesol (FAR) is an acyclic sesquiterpene alcohol found in many natural sources including vegetables, fungi, fruits and herbs with demonstrated antimicrobial, antiproliferative, antiallergic, and anti-inflammatory properties (Wu et al., 2019). Previous studies have demonstrated that its antibacterial action against *S. aureus* was attributed to two mechanisms, the alteration of bacterial membranes and the inhibition of the mevalonate pathway (Kaneko et al., 2011). It was found that in combination with topical antibiotics, FAR at concentrations below the minimum inhibitory concentration (MIC) was able to restore the activity of methicillin and oxacillin on *S. aureus* MJMC102 and MJMC111 strains, as well as against two other methicillin-resistant *S. aureus* (MRSA) clinical isolates, and potentiated the effect of fusidic acid, mupirocin, and gentamicin (Oliveira et al., 2022). FAR has also been evaluated against biofilms formed by different microorganisms restraining the formation of single or multiple biofilms of *Candida albicans* ATCC 10 231 and *Streptococcus mutans* ATCC 25 175 strains (Fernandes et al., 2018). In biofilms formed from MRSA, FAR reduced viability, disrupted the plasma membrane, and showed synergism with gentamicin (Barot et al., 2020). Most of the studies show encouraging results on the use of FAR as an alternative treatment for bacterial biofilms; however, its high lipophilicity and low water solubility (logP = 4.84) (Valcourt et al., 2021) hamper its widespread use in the clinical practice due to its reduced bioavailability. In order to solve this limitation, FAR has been encapsulated or loaded into different carriers. For example, inorganic materials such as halloysite (Barot et al., 2020) and amorphous silica (Sousa et al., 2012) and organic ones such as poly (lactic-*co*-glycolic acid) (PLGA) (Yenice Gürsu, 2020) and chitosan (Fernandes Costa et al., 2018) have been also used to encapsulate FAR. Non-ionic copolymer surfactants such as Pluronic®-based micelles, which dissolve and readily disperse the hydrophobic FAR in water have also been used to promote aqueous solubility and have shown high levels of *Streptococcus mutans* biofilm inhibition (Nowacka et al., 2020). Valcourt *et al.* (Valcourt et al., 2021) have demonstrated that FAR formulated as lipid NPs restored the sensitivity of *Escherichia coli* MCR-1 to colistin, allowing a reduced concentration of this last-resort antibiotic to obtain bactericidal effects. Moreover, FAR may have positive effects on wound healing because it can reduce oxidative stress and inflammation (Wu et al., 2021). For example, liposomal FAR has shown restorative wound healing improvements *in vitro* and *in vivo* after third-degree burns (Wu et al., 2019).

Not only active substances derived from essential oils are used for controlling pathogenic topical microorganisms, but also antiseptics act against a wide spectrum of micro-organisms, including bacteria, fungi, viruses, protozoa, and even spores (Rueda-Fernández et al., 2022). Chlorhexidine (CHXD) is considered the "gold standard" antiseptic being active against gram-positive/gram-negative bacteria, facultative anaerobes/aerobes, molds, yeasts and viruses. It exhibits both immediate and residual excellent antimicrobial effects, preventing further re-colonization by microorganisms on the skin (Agarwal et al., 2012). It has been used in combination therapy, for example, combinations of CHXD with the antibiotic ciprofloxacin demonstrated synergetic effects (Pietsch et al., 2021). The synergetic effect between tea tree oil with CHXD on the antimicrobial activity against *E. coli* was shown to be prominent (Pietsch et al., 2021). However, to the best of our knowledge, there are no previous reports describing the *in vivo* synergism between CHXD and FAR during the treatment of infected topical wounds.

The aim of the present study is to focus our efforts on the evaluation of the bactericidal and antibiofilm activity of the natural compounds THY and FAR-based nanoparticles (NPs) and the antiseptic CHXD against bioluminescent *S. aureus*. This *S. aureus* Xen36 bioluminescent bacterial strain was used to allow real-time *in vivo* monitoring of infection progression and antimicrobial treatment outcome monitoring by means of an IVIS® bioluminescence imaging system. We hypothesized that the combination of different agents with different mechanisms of antimicrobial action may act synergistically (i.e., the combined antimicrobial effect of those different agents is superior to the expected additive effect of said agents) by targeting multiple sites in bacteria, hence broadening the spectrum of antibacterial action. In this regard, the combinations of CHXD with THY, CHXD with FAR NPs, and THY with FAR NPs, were tested against planktonic and sessile forms of the bacterium. Moreover, THY-loaded electrospun Eudragit® S100-based dressings (S100-THY) were also evaluated both *in vitro* and *in vivo* against an experimental topical infection with *S. aureus* Xen36. We postulate a novel clinical protocol in which the regular treatment of infected wounds with a topical antiseptic (e.g., CHXD) would be combined with a terpene-loaded wound dressing to achieve a complete bacterial eradication and a successful wound care. We have previously developed advanced drug eluting dressings containing antimicrobials and we have validated them *in vitro* (Miranda-Calderon et al., 2022) and *in vivo* (Gámez-Herrera et al., 2020). In this current work, we have gone one step further by using a bioluminescent bacterial strain to allow us to perform real-time *in vivo* monitoring of infection progression and to improve the antimicrobial treatment outcome. We have been able to monitor how the bacterial community colonized the wound and how our advanced dressings reduce their viability by measuring their metabolic bioluminescence emitted analyzing planktonic and sessile bacterial modes of growth. In addition, we have evaluated, as a novelty, the natural antiseptic terpenes thymol and farnesol standing alone or in combination with the standard care antiseptic chlorhexidine.

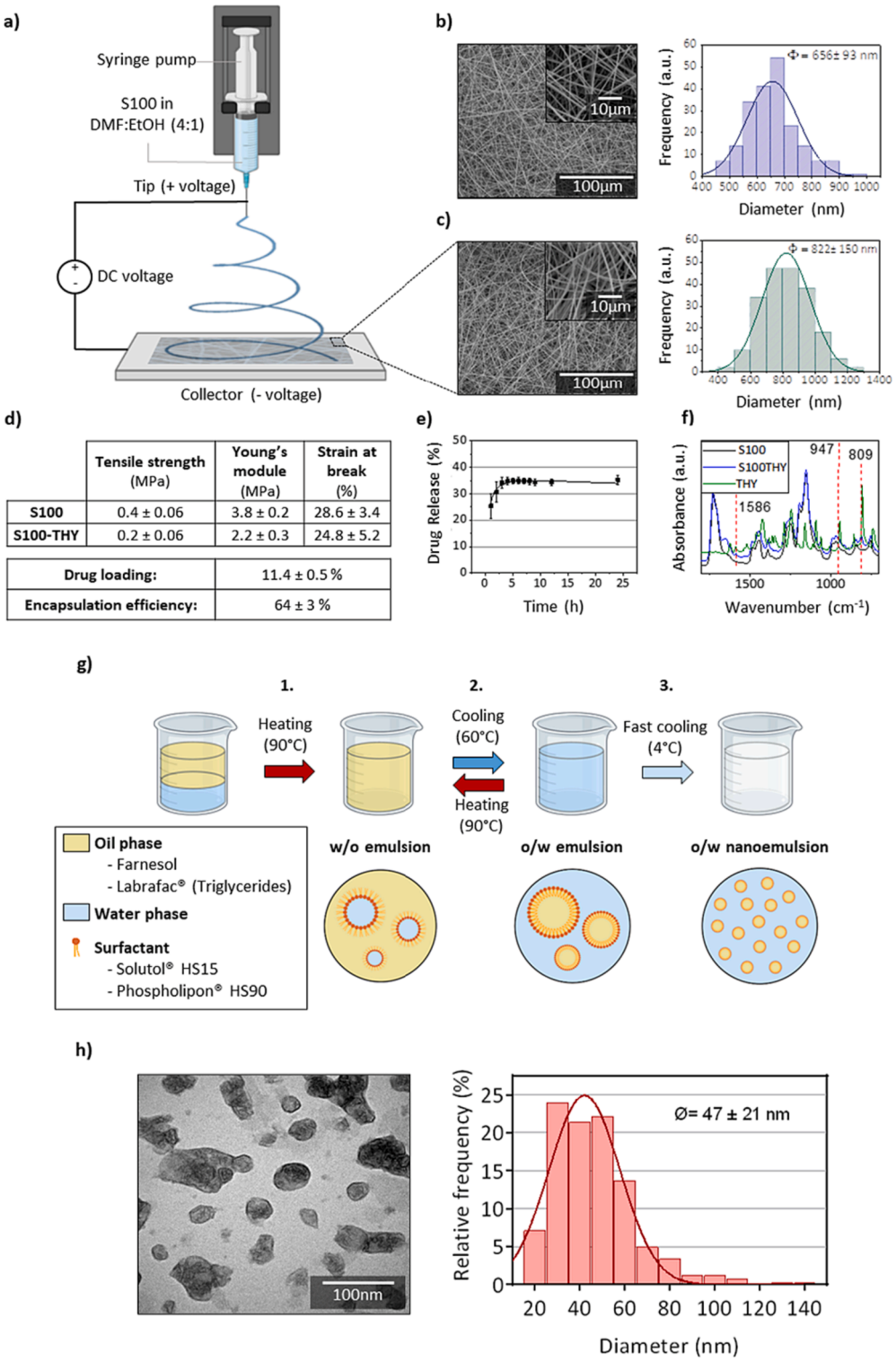

	Tensile strength (MPa)	Young's module (MPa)	Strain at break (%)
S100	0.4 ± 0.06	3.8 ± 0.2	28.6 ± 3.4
S100-THY	0.2 ± 0.06	2.2 ± 0.3	24.8 ± 5.2

Drug loading:	11.4 ± 0.5 %
Encapsulation efficiency:	64 ± 3 %

Fig. 1. Synthesis and characterization of antimicrobial formulations. (a) Scheme depicting the S100 and S100-THY fibers synthesis by electrospinning. (b) SEM images and size distribution histogram of S100-THY fibers. (c) SEM images and size distribution histogram of S100 fibers. (d) Mechanical properties of S100 and S100-THY fibers and drug loading and encapsulation efficiency of THY in S100-THY fibers. (e) Kinetic release profile of THY from S100-THY fibers. (f) FTIR spectra of THY, S100 and S100-THY fibers. (g) Scheme showing the synthesis of FAR nanoparticles by simple emulsion with the phase inversion temperature (PIT) cycling method. (h) TEM image of FAR NPs and particle size distribution histogram.

2. Materials and methods

The supplementary materials and methods and any associated references are available in Supplementary Materials section.

2.1. Synthesis and characterization of S100-THY fibres

A S100 solution (30 % w/v) was prepared by dissolving the polymer in a mixture of DMF (dimethylformamide) and EtOH (ethanol) in a proportion of 4:1. For the preparation of THY loaded fibers, THY was

added to the previous solution to obtain a concentration of 20 % w/w (referred to the polymer weight). The solution was loaded in a syringe connected to a Yflow 2.2 D500 electrospinner (Electrospinning Machines/R&D Microencapsulation, Málaga, Spain), equipped with a rotating drum collector. The distance between the tip of the needle and the collector was fixed at 15 cm, and the solution flow rate was 1.0 mL/h. The negative voltage applied was varied in the range of −3.02 to −3.69 kV and the positive one varied from +13.15 to +15.07 kV.

The morphology of the synthesized fibers was analyzed by scanning electron microscopy (SEM) using an Inspect F50 FEG scanning electron microscope (FEI company, Hillsboro, USA). Nanofiber diameters were measured (N = 200) using the DigitalMicrograph® software (Version 2.31.734.0; Gatan, Pleasanton, USA).

Mechanical properties of the S100 and S100-THY fibers were evaluated by means of a tensile test carried out at room temperature in an Instron Microtester 5548 and a video extensometer laser (1 mm/min, 1 KN load cell; Instron, Norwood, USA). The tested probes (N = 5) followed the ISO 527-1:2012 norm (Plastics: Determination of tensile properties) being cut into 50 mm × 5 mm strips. A full-scale load of 20 N and maximum extension of 100 mm were employed.

THY drug loading was determined by GC-MS using a Shimadzu 2010SE GC-MS chromatograph (Kyoto, Japan) equipped with a Zebron ZB-50 capillary (Phenomenex, Torrance, USA). The encapsulation efficiency (EE) and the drug loading (DL) were calculated with Eqs. (1) and (2), respectively:

$$EE(\%) = \frac{mass\ of\ entrapped\ drug\ (mg)}{mass\ of\ drug\ added\ (mg)} x100 \quad (1)$$

$$DL(\%) = \frac{mass\ of\ entrapped\ drug\ (mg)}{Total\ mass\ of\ nanofibers\ (mg)} x100 \quad (2)$$

Fourier-transform infrared (FTIR) spectra were recorded using a Bruker VERTEX 70 FTIR spectrometer (Bruker, Billerica, USA) equipped with a Golden Gate® diamond ATR accessory. Spectra were recorded by averaging 40 scans in the 4000–600 cm^{-1} wavenumber range at a resolution of 4 cm^{-1} after baseline correction and water vapor subtraction.

2.2. Thymol release studies

THY release from the S100-THY fibers was carried out using a J.P. Selecta Movil-Rod rotating shaker placed inside an incubator (37 °C). Five mg of S100-THY (N = 5) were immersed in 5 mL of PBS (pH 7.4) (sink conditions) during 24 h under orbital stirring (60 rpm). At predetermined time intervals, 1 mL of the supernatant was collected and an equal volume of fresh solution was replenished. The collected samples were analyzed in an Acquity UPLC Waters liquid chromatography system (Waters, Milford, USA). An Acquity UPLC Waters BEH C18 column was employed for the THY detection. As internal standard, 25 ppm of naproxen were included in the samples.

2.3. Synthesis and characterization of farnesol loaded nanoparticles

Farnesol lipidic nanoparticles (FAR NPs) were prepared following the method depicted by Valcourt *et al.* [25]. In brief, the oily phase made of FAR (460 g) and caprylic/capric acid triglycerides (69 % w/w) was mixed under magnetic stirring with a 0.5 M NaCl aqueous solution containing two surfactants, Solutol® HS15 (28.4% w/v) and Phospholipon® HS90 (2.52 % w/v). The initial oil-in-water emulsion was heated over the phase-inversion temperature (PIT, 90 °C) to obtain a water-in-oil emulsion. Then, it was cooled down below the PIT at 60 °C at which it reverted to the oil-in-water emulsion initial state. Three of those temperature cycles were completed until the oil-in-water framework was fixed by adding 12 mL of water at 4 °C.

Size distribution of synthesized FAR NPs was determined using a NanoSight NS300 (Malvern Panalytical, Madrid, Spain). Size and morphology were also studied by transmission electron microscopy (TEM). For TEM sample preparation, 20 μL of the suspension were deposited on a carbon-coated copper grid and dried at room temperature. TEM images were recorded on a FEI Tecnai T20 transmission electron microscope (FEI, Oregon, USA) operating at 200 kV.

2.4. Biological tests

In vitro antimicrobial activity tests of drugs, *in vitro* antimicrobial activity of S100-THY, *in vivo* wound infection studies, wound infection evaluation and pathological studies as well as statistical analyses are described in the supplementary information.

3. Results and discussion

3.1. Characterization of electrospun S100-THY fibres and farnesol nanoparticles

Fig. 1a–c depicts the setup and synthesis conditions to produce electrospun fibers, as well as the SEM analysis and diameter histograms. Homogeneous bead-free S100-THY fibers with a mean diameter of 656 ± 93 nm were obtained (Fig. 1b). Bare unloaded S100 fibers displayed slightly different mean diameter (822 ± 150 nm; Fig. 1c). These results were close to those reported previously for Eudragit® S100 fibers obtained by monoaxial electrospinning and loaded with benzoic acid or 9-anthacen carboxylic acid (500–600 nm) (Burgess et al., 2018) or with budesonide, which also showed uniform structure with a mean diameter of 660 nm (Turanlı and Acartürk, 2021).

THY encapsulation efficiency achieved in the S100 fibers was 64 ± 3 wt.%, which gives a drug loading of 11.4 ± 0.5 wt.% of THY (Fig. 1d). Burgess *et al.* (Burgess et al., 2018) have shown that the encapsulation efficiency for different active compounds in electrospun S100 fibers could be higher than 85 wt.%, however, the drug loading was always lower than 10 % w/w. Those authors attributed the decrease in the loading efficiency to losses of the corresponding active compounds during the electrospinning through small amounts of precipitation or adherence to the syringe walls. In addition, due to the high volatility of THY (0.016 mm Hg at 25 °C), probably part of the active compound is evaporated together with the solvent (DMF:EtOH) in the electrosprayed jet formed from the needle tip to the collector plate. Data described in Fig. 1d show that the electrospun dressings are not mechanically rigid but rather weak and easily conformable to the wound which is positive because dressings should be easy to apply, adaptable, conformable and porous being permeable to allow gas exchange while avoiding wound maceration. The mechanical property analysis of empty S100 fibers did not reveal significant differences compared to those observed for S100-THY fibers. As shown in Fig. 1d, the inclusion of THY in the dressing slightly reduces its resistance to elastic deformation, therefore, the drug loaded dressing is mechanically similar but shows lower stiffness and higher elasticity than its parent non loaded dressing. Still, this high elasticity makes the resulting dressings soft and easily conformable to the wound contour.

Kinetic studies (Fig. 1e) confirmed that 35 % of the loaded THY was released in the first 5 h. An initial burst release was observed which could be associated to the presence of THY on the external surface of the fibers as previously reported (Garcia-Salinas et al., 2020; García-Salinas et al., 2020b; Ramamoorthy and Rajiv, 2015). Then, a controlled diffusion over 5 h reaching 35 % of the loaded THY was achieved in accordance with previous studies regarding S100 sustained drug delivery (Sun et al., 2022) as well as THY release from different polymeric fibers including S100 (García-Salinas et al., 2020b; Miranda-Calderon et al., 2022; Sun et al., 2022). Therefore, our proposed system would produce an extended duration of action being the THY released in a controlled manner.

S100-THY, S100 and THY FTIR spectra in the 1800–700 cm^{-1} region are shown in Fig. 1f. Spectrum of loaded fibers displayed all the characteristics bands of S100, however, the presence of THY was confirmed

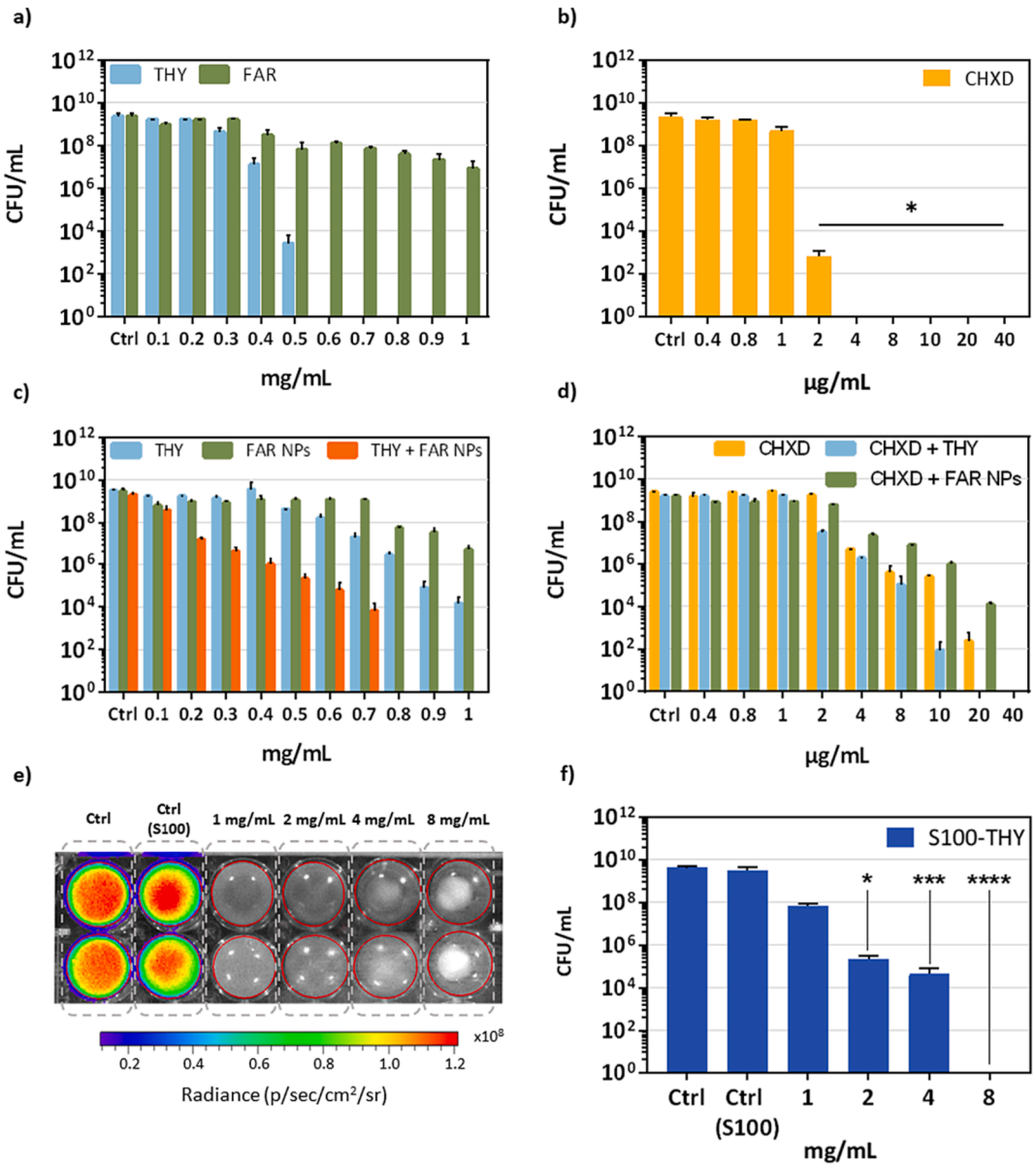

Fig. 2. *In vitro* antimicrobial activity of the different treatments evaluated. a) *S. aureus* Xen36 growth in planktonic state treated with free THY and FAR NPs. b) *S. aureus* Xen36 in planktonic state treated with CHXD. c) Antimicrobial activity of THY, FAR NPs and the combination of both at the same concentration on *S. aureus* Xen36 mature biofilms. d) Antimicrobial activity of CHXD alone and in the presence of a fixed concentration of THY (0.5 mg/mL) and FAR NPs (1 mg/mL) on *S. aureus* Xen36 biofilm. e) Bioluminescence signal of *S. aureus* Xen36 in solid agar after 24 h of treatment with different S100-THY fiber concentrations. f) Bacterial colony counts of the cultures depicted in e). Data are expressed as Mean ± SD of three experiments evaluated separately. Statistics compare each treatment *vs* the control group ($^{*}p < 0.05$; $^{**}p < 0.01$; $^{***}p < 0.001$; $^{****}p < 0.0001$).

by the vibrations observed at 809, 947 and 1586 cm^{-1}. This last band can be assigned to the phenol ring of THY, while peaks detected at 809 and at 947 cm^{-1} would be related to out of plane aromatic C–H waging and bending vibrations that in the THY spectrum appear at 804 and 943 cm^{-1}, respectively (Dikić et al., 2021; Milovanovic et al., 2016). The observed slight blue shift in the loaded fibers could indicate some interactions between THY and the polymer which is a positive outcome because those supramolecular interactions will contribute to slow down the release of the active compound. Considering the chemical structure, the interaction could be expected between the hydroxyl groups of THY and the carbonyl groups of the polymer. This interaction would be confirmed by the change in the intensity ratio between the characteristic C═O stretching of the S100 esterified carboxylic group observed at 1725 cm^{-1} and the shoulder due to carboxylic acid groups (1650 cm^{-1}) (Liu et al., 2018). This supramolecular interaction between the polymer and the essential oil may also explain the sustained release observed in the THY release studies described above (Fig. 1e).

The process to synthesize FAR NPs is depicted in Fig. 1g which involved a simple emulsion with the phase inversion temperature (PIT) cycling method (Valcourt et al., 2021). TEM images of individual FAR NPs (Fig. 1h) showed a mean diameter of 47 ± 21 nm. On the other hand, most of the particles exerted a hydrodynamic diameter of 89 ± 44 nm, even though some agglomerates of more than 100 nm were observed. This hydrodynamic diameter was slightly larger than that previously reported by Valcourt *et al.* for the same NPs (Valcourt et al., 2021). Farnesol and FAR NPs FTIR spectra were measured but the overlapping observed for both systems together with the vibrational signals assigned to Labrafac®, Solutol® and Phospholipon® made impossible to discriminate between the corresponding signals in the 4000–500 cm^{-1} region (results not shown).

3.2. In vitro bactericidal activity

The antimicrobial efficiency of the compounds and materials tested against *S. aureus* Xen36 is depicted in Fig. 2 and in the supplementary information section (Fig. S2).

Bactericidal effects of THY, FAR NPs and CHXD in planktonic cultures demonstrated differential effects regarding the treatment applied (Fig. 2a, 2b, S2). Colony counting experiments (Fig. 2a and b) revealed that CHXD was the most effective antimicrobial compound tested showing a MIC of 2 μg/mL whereas THY and FAR NPs significantly inhibited bacteria growth at concentrations of 0.4 and 0.9 mg/mL, respectively. In this line, the concentration needed to reach the minimum bactericidal concentration (MBC) was higher for THY (0.6 mg/mL) than for CHXD (4 μg/mL), and planktonic cultures treated with FAR NPs were not totally eradicated even at the highest concentration assayed (1 mg/mL). Indeed, at this concentration, only a 2-log reduction was observed with FAR NPs, demonstrating the reduced effectiveness of FAR NPs *vs* THY and CHXD. Bioluminescence evaluation of the treated cultures also showed a high efficiency of the compounds tested in the inhibition of bacterial growth displaying a clear dose-dependent effect (Fig. S2). Luminescence signal intensity (LSI) was depicted by normalizing the data of the relative light units (RLU) acquired from the cultures, considering the average of RLU at time zero as LSI = 1. CHXD treatment significantly decreased the bioluminescence at a concentration of 1 μg/mL since the first hour after CHXD addition. On the other hand, THY and FAR NPs achieved a significant reduction in the bioluminescence after the first hour of treatment at 0.6 and 0.1 mg/mL, respectively. Surprisingly, even though FAR NPs did not reduce the bacterial cell counts in more than 2-log when treated with 1 mg/mL, bioluminescence was clearly arrested at a much lower concentration (0.1 mg/mL). This observation has also been reported by others for the same strain where the antimicrobial pressure strongly impacts the relationship between CFU and bioluminescence (Daghighi et al., 2015). Those authors conclude that under the presence of antimicrobials bioluminescence is not controlled by luxA expression but by co-factors impacting the bacterial metabolic activity. Bioluminescence depends mainly on two elements, the concentration of bacteria and their metabolic activity (since ATP is needed to produce light). Also, a decrease in bioluminescence without a decrease in the number of bacteria strongly suggests that FAR NPs at a concentration as low as 0.1 mg/mL reduce the metabolic activity of *S. aureus*.

The effects of the treatment of *S. aureus* Xen36 biofilm with these compounds and also with the different combinations assayed showed promising results particularly concerning the combined administration of these compounds (Fig. 2c, 2d and S2). In general, biofilm eradication required higher compound concentration, as resistance and tolerance to antimicrobials is known to be increased compared to planktonic cultures owing to extracellular polysaccharide (EPS) matrix impairing antibiotic diffusion and reduced metabolic state (dormancy) (Hall and Mah, 2017). Our results demonstrated that CHXD treatment reached again the lowest biofilm bactericidal concentration (BBC) (4 μg/mL) and minimal biofilm eradication concentration (MBEC) (40 μg/mL) values whereas the total eradication of bacterial biofilms at the highest concentrations tested for THY and FAR NPs was not achieved. Regarding the bioluminescence signal (Fig. S2), biofilms treated with CHXD also displayed a significant reduction of their signal in the first hour of treatment at BBC (4 μg/mL). However, THY (≥0.6 mg/mL) and FAR NPs (≥0.1 mg/mL) were able to reduce LSI through a more sustained trend and particularly, in the case of THY, the signal was recovered to the control levels after 12 h.

Interestingly, some of the combined treatments assayed (THY + FAR NPs, CHXD + THY, CHXD + FAR NPs) involved an enhanced bactericidal effect. Specifically, THY + FAR NPs significantly reduced the BBC value (0.2 mg/mL; >70 % reduction *vs* THY and FAR NPs independently tested) and the MBEC was attained at 800 μg/mL (Fig. 2c). The addition of THY to CHXD treatment resulted in a decrease by half the CHXD MIC and MBC values. However, the addition of FAR NPs to CHXD did not involve any change in bacterial growth (Fig. 2d).

S100-THY fibers were also evaluated in solid cultures in order to elucidate their potential *in vitro* antimicrobial effects against *S. aureus* Xen36 (Fig. 2e and 2f). Bioluminescence measurements (Fig. 2e) pointed to a significant effect of the electrospun loaded nanofibers which was confirmed in the colony cell counts (Fig. 2f). MIC was attained at 1 mg/mL whereas MBC at 8 mg/mL which correlates with a THY released concentration of 0.04 mg/mL and 0.32 mg/mL, respectively. These results are significantly lower than those obtained for the planktonic and biofilm experiments when free THY was added to the cultures. MIC and MBC values were depleted more than 90 % when THY was loaded into S100 fibers compared to the treatment with free THY. These promising data agree with our previous studies (García-Salinas et al., 2020b; Gracia et al., 2018), highlighting the relevance of drug encapsulation to obtain a time-controlled sustained release due to the polymer chemical modification, as well as the need of contact between electrospun fibers and bacteria to yield a significant antimicrobial effect reducing the drug concentration required. The shiny white contrast observed in the wells containing dressings at 8 mg/mL concentration is caused by the large number of piled dressings needed to reach such high concentration causing a height increase, a change in the working distance, and its corresponding white contrast in the IVIS® equipment.

Considering these *in vitro* studies, CHXD was the most effective treatment in the reduction of bacteria viability, both in planktonic and biofilm cultures. However, once the biofilm is formed, the combination of THY together with CHXD or FAR NPs produced and enhanced antimicrobial effect, showing a reduction in BBC and MBEC values higher than 50 %. In addition, S100-THY loaded fibers also demonstrated a superior *in vitro* efficiency for the encapsulated THY *vs* the equivalent doses of the free compound.

Other authors have previously shown the higher bactericidal effects of CHXD *vs* THY (Karpanen et al., 2008). For instance, previous MIC and MBC values obtained when CHXD was added to planktonic and biofilm cultures of *S. epidermidis* were in the range of our results (2–16 μg/mL) while THY was needed at higher concentrations (0.5–16 mg/mL) to inhibit or eliminate the same bacteria. However, their results did not show an increased antimicrobial effect with the combined use of CHXD and THY as our studies did. Different studies have suggested that the enhanced antimicrobial activity of the combined treatment of CHXD with terpene-derived compounds, as THY and farnesol are, might be attributed to the combined action on the same bacterial target (i.e., cell membrane) (Filoche et al., 2005). In addition, CHXD biofilm disruption may be boosted due to its cationic character and the mostly negative charge of the biofilm extracellular matrix. The combination of CHXD and terpene-derived compounds would have both hydrophobic and hydrophilic features and may modify the ionic interactions with the biofilm extracellular matrix (Karpanen et al., 2008).

Conversely, previous studies have suggested the potential interaction of FAR with the bacteria membrane as well as with the *quorum sensing* system of the bacteria (Inoue et al., 2004; Jabra-Rizk et al., 2006; Sato et al., 2004), showing antimicrobial activity for FAR NPs. Specifically, its hydrophobicity fostered FAR accumulation in the bacteria membrane and thus, promoted cell leakage (Jabra-Rizk et al., 2006; Togashi et al., 2010). Moreover, FAR was reported as a modifier of the synthesis of glucan, a biofilm matrix polysaccharide, inhibiting the accumulation of biofilm biomass (Koo, 2003). However, the concentrations of FAR (20–250 μg/mL) and the bacteria strains used in these previous studies are varied, hindering to ascertain a general trend for different microorganisms and should be considered on a case-by-case basis. In this regard, some authors have highlighted the potential of FAR to be used as a sensitizer in combination with different antimicrobials by changing the bacteria membrane permeability, pointing to this strategy as one more efficient compared to its role in monotherapy (Bandara et al., 2016; Jabra-Rizk et al., 2006). This mechanism may promote the influx of antimicrobial compounds into the cell, enhancing the interaction with intracellular targets. Therefore, the combined used in the treatment of

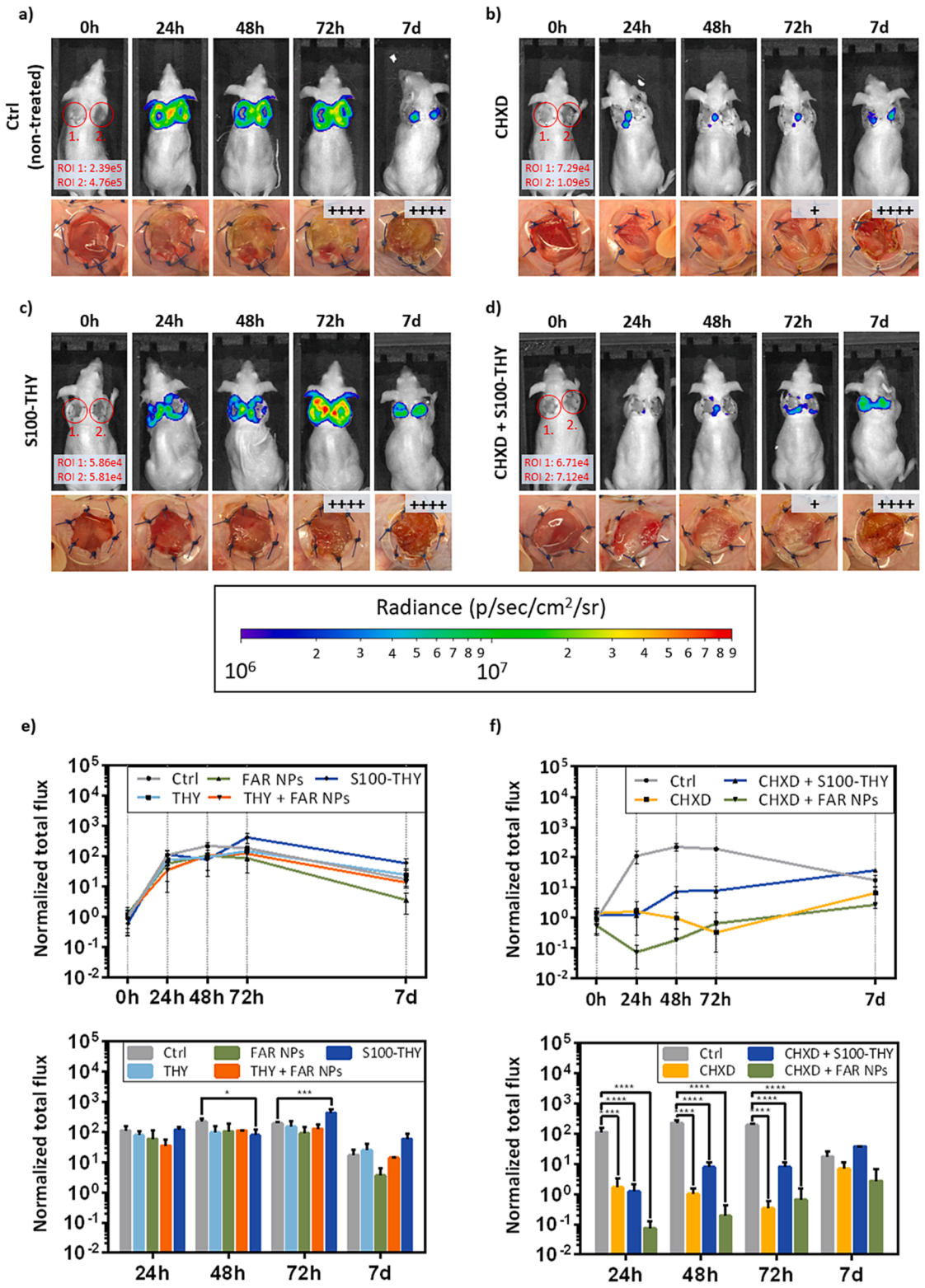

Fig. 3. *In vivo* evaluation of *S. aureus* Xen36 infected and treated wounds in SKH1 mice at 24, 48, 72 h and 7 days PSI. (a-d) Bioluminescent signal, morphology and microbiological analyses of the wounds. Each wound of every animal is a region of interest (ROI). The values of total flux at ROIs that are out of scale are indicated in red in the corresponding image. Microbiological results regarding bacteria colony counting are shown as insets from (+) low number of colonies to (++++) massive culture. (a) Control group (infected, non-treated). (b) Infected and treated with CHXD. (c) Infected and treated with S100-THY dressing. (d) Infected and treated with CHXD and S100-THY dressing. (e-f) Changes in bioluminescent signal of *S. aureus* Xen36 obtained from the different experimental groups assayed. Upper graphs show the evolution of the bioluminescent signal (total flux) at ROIs over time. Data are normalized to the average initial signal (0 h PSI). Bottom graphs show data comparison between groups at each time point. Data are expressed as Mean ± SD of three independent experiments. Statistics compare each treatment *vs* the control group ($^{*}p < 0.05$; $^{**}p < 0.01$; $^{***}p < 0.001$; $^{****}p < 0.0001$).

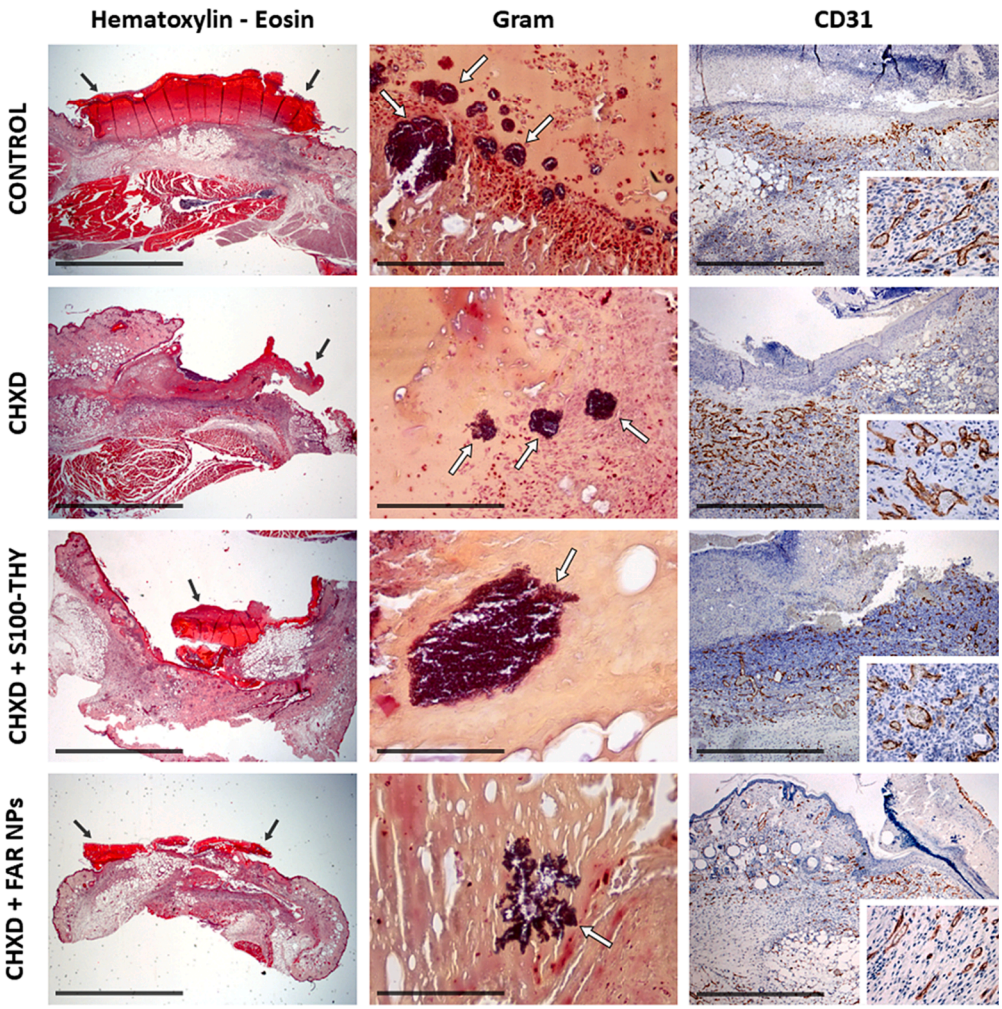

Fig. 4. Histopathology from representative mice groups: Control group (not treated), CHXD, CHXD + S100-THY, CHXD + FAR NPs. Lesions are similar in all cases, with a marked serocellular crust formation (black arrows). Bacteria are present in all groups, only within the crust (white arrows). Neovascularization (labelled in brown color in all images and insets) may be less intense in CHXD-FAR NPs group. Haematoxylin – Eosin, bar = 4 mm; Gram, bar = 100 μm; and CD31, bar = 1 mm; insets at 10x.

mature bacterial biofilms of FAR NPs with THY, which in our *in vitro* studies involved a reduction in the MIC value up to 70 %, could be a promising strategy to effectively eradicate biofilms in the treatment of infected wounds.

3.3. *In vivo studies*

The *in vivo* effectiveness of the antimicrobial treatments assayed in this study was evaluated in a murine excisional wound splinting model following the methodology described in Fig. 1. Different control and experimental groups were performed as detailed in section 2.3 S.I. The effects of the proposed treatments were determined by the simultaneous measurement of the bioluminescence signals emitted by the bacteria present in the wounds, the microbiological analysis of the wounds, and the histopathological studies.

Fig. 3 and Fig. S3 show the results obtained regarding the bioluminescent signal, wound morphology and microbiological analyses. These results confirmed the superior efficiency of the treatments containing CHXD as the *in vitro* experiments revealed. Seventy-two h after surgery and infection, moment in which wounds were left uncovered and untreated up to 7 days PSI, the groups treated daily with CHXD, CHXD + FAR NPs, and CHXD + S100-THY, depicted a significant decrease in the bioluminescence signal and concomitantly, in the bacterial counts. Moreover, among the other experimental groups assayed, FAR NPs displayed a slightly higher bactericidal activity compared to those of THY and S100-THY groups (Fig. 3e). It should be noted that 7 days PSI, no significant differences among groups were reported owing to the interruption of the treatments and because we uncovered the wounds 72 h after infection. It is important to point out the tremendous bacterial load that constituted the initial experimental infection performed on each wound (2.5×10^5 CFU/wound). We observed that compared to the treatments, the bacteria easily proliferated on the control animals (non-treated) (Fig. 3a) and later on, the animals immune system together with the scabbing process and the drying caused after removing the covering made the bacterial burden to reduce at 7 days. But considering that all the bacteria are not eliminated, they proliferated and the bacterial cell counts showed still high burden. The initial bacterial challenge in the case of the treated animals (Fig. 3b and c) was clearly reduced in the first days, but after uncovering the wounds and quit treating, the bacteria continued proliferating as expected. We hypothesize that in a real clinical setting and considering the aseptic conditions and practices in surgery rooms, any accidental bacterial load will be minimal and the proposed treatments would be able to completely eliminate all bacteria present preventing early postwounding infections. Fig. 3c shows that the antimicrobial wound dressing was unable to reduce the initial burden due to its delayed antimicrobial release, but when combined with the immediately available antiseptic CHDX (Fig. 3d) the bacterial load was largely reduced.

Histopathological and immunohistochemical evaluations were performed to stablish the wound status regarding changes in the tissue morphology, infection, and angiogenesis (Fig. 4). The representative groups analyzed were those treated with CHXD and its combinations as these were the most effective in both *in vitro* and *in vivo* studies. Regarding inflammation and changes in tissue morphology, lesions observed in all groups were similar. Moreover, coccoid bacteria were also detected restricted to the surface of the wounds. Neovascularization revealed by CD31 immunohistochemistry displayed a slightly lower signal in the CHXD + FAR NPs treated group which may suggest a slower tissue regeneration compared to CHXD and CHXD + S100-THY groups. CHXD and its combinations with the natural terpenes here tested contributed to a successful reduction in the infective bacterial load present with no severe damage to the tissues. Granular tissue formation, re-epithelialization, remodeling and scar tissue formation were successful in the treated groups.

Considering our *in vitro* and *in vivo* results, and that the most common treatment in the clinical practice for eradicating chronic biofilm infections is the antiseptic cleansing, debridement and the continuous administration of systemic or topical antibiotics depending on the wound culture results, the concomitant use of our proposed treatments may involve a significantly higher efficacy (Gámez-Herrera et al., 2020).

4. Conclusion

In this work, different treatments based on the bactericidal and antibiofilm ability of the terpene compounds THY and FAR NPs, and the antiseptic CHXD, were evaluated in depth both *in vitro* and *in vivo*. Our *in vitro* results pointed to a significant bactericidal activity of those treatments which include the antiseptic CHXD but also the combination of different treatments demonstrated an improved bactericidal efficiency over monotherapy. There is no a direct correlation between the bacterial cell counts and the bioluminescence emitted by *S. aureus* Xen36 under the presence of the antimicrobial treatments, probably because other cofactors impact the bacterial metabolic activity. The *in vivo* study confirmed the *in vitro* results, highlighting the potential use of CHXD together with terpene-based compounds for a better wound treatment and enhanced healing. We have shown *in vitro* that combination therapies outperform monotherapy using equivalent doses of the corresponding antimicrobial compounds. *In vivo*, the treatments initially showed a large bacterial reduction but because no all the pathogenic microorganism was completely eliminated, after treatment cessation, remaining bacteria were able to regrow. The exponential increase of *S. aureus* resistant infections and the prevalent presence of these biofilm-forming strains point out to the critical need for the development of novel approaches in which the combination of different bactericidal compounds may be the key event to improve current treatments in infected wound management.

CRediT authorship contribution statement

Guillermo Landa: Data curation, Formal analysis, Investigation, Methodology, Software, Validation, Writing – original draft, Writing – review & editing. **Laura G. Miranda-Calderon:** Data curation, Formal analysis, Investigation, Methodology, Writing – review & editing. **Alex Gomez:** Data curation, Formal analysis, Investigation, Methodology, Writing – review & editing. **Marta Perez:** Data curation, Formal analysis, Investigation, Methodology, Writing – review & editing. **Victor Sebastian:** Data curation, Formal analysis, Investigation, Methodology, Writing – review & editing. **Manuel Arruebo:** Conceptualization, Formal analysis, Funding acquisition, Investigation, Project administration, Resources, Supervision, Validation, Writing – original draft, Writing – review & editing. **Isabelle Lamarche:** Data curation, Formal analysis, Investigation, Methodology, Writing – review & editing. **Frederic Tewes:** Conceptualization, Data curation, Formal analysis, Funding acquisition, Investigation, Methodology, Supervision, Visualization, Writing – review & editing. **Silvia Irusta:** Conceptualization, Formal analysis, Funding acquisition, Investigation, Project administration, Resources, Supervision, Validation, Writing – original draft, Writing – review & editing. **Gracia Mendoza:** Formal analysis, Investigation, Supervision, Validation, Visualization, Writing – original draft, Writing – review & editing.

Declaration of Competing Interest

The authors declare that they have no known competing financial interests or personal relationships that could have appeared to influence the work reported in this paper.

Data availability

Data will be made available on request.

Acknowledgments

The authors acknowledge the Spanish Ministry of Science and Innovation (grant number PID2020-113987RB-I00) for funding. This manuscript is also the result of the project PDC2021-121405-I00, founded by MCIN/AEI/10.13039/501100011033 and by the European Union "NextGenerationEU"/PRTR. We also thank the LMA-INMA (University of Zaragoza, Spain), the Histopathology Unit from CNIO (Spain), and Pathological Anatomy Core Unit from IACS/IIS Aragon for their instruments and expertise. This work has benefited from the facilities and expertise of PREBIOS platform (Université de Poitiers, France). G.L. acknowledges the support from the FPI program (PRE2018-085769, Spanish Ministry of Science, Innovation and Universities). L.G.M-C. acknowledges funding from the Mexican Council of Science and Technology (CONACyT) through doctoral grant #710618. G.M. gratefully acknowledges the support from the Miguel Servet Program (MS19/00092; Instituto de Salud Carlos III). CIBER-BBN is an initiative funded by the VI National R&D&i Plan 2008-2011 financed by the Instituto de Salud Carlos III with the assistance of the European Regional Development Fund. A portion of the images depicted in figures 1 and S1 were created with the assistance of BioRender.com.

Appendix A. Supplementary data

Supplementary data to this article can be found online at https://doi.org/10.1016/j.ijpharm.2023.123502.

References

Agarwal, A., Nelson, T.B., Kierski, P.R., Schurr, M.J., Murphy, C.J., Czuprynski, C.J., McAnulty, J.F., Abbott, N.L., 2012. Polymeric multilayers that localize the release of chlorhexidine from biologic wound dressings. Biomaterials 33, 6783–6792. https://doi.org/10.1016/j.biomaterials.2012.05.068.

Bandara, H.M.H.N., Herpin, M.J., Kolacny, D., Harb, A., Romanovicz, D., Smyth, H.D.C., 2016. Incorporation of Farnesol significantly increases the efficacy of liposomal ciprofloxacin against *Pseudomonas aeruginosa* Biofilms *in Vitro*. Mol. Pharm. 13 (8), 2760–2770. https://doi.org/10.1021/acs.molpharmaceut.6b00360.

Barot, T., Rawtani, D., Kulkarni, P., Hussain, C.M., Akkireddy, S., 2020. Physicochemical and biological assessment of flowable resin composites incorporated with farnesol loaded halloysite nanotubes for dental applications. J. Mech. Behav. Biomed. Mater. 104, 103675 https://doi.org/10.1016/j.jmbbm.2020.103675.

Burgess, K., Li, H., Abo-Zeid, Y., Fatimah, W.G.R., 2018. The effect of molecular properties on active ingredient release from electrospun eudragit fibers. Pharmaceutics 10, 103. https://doi.org/10.3390/pharmaceutics10030103.

Daghighi, S., Sjollema, J., Harapanahalli, A., Dijkstra, R.J.B., van der Mei, H.C., Busscher, H.J., 2015. Influence of antibiotic pressure on bacterial bioluminescence, with emphasis on Staphylococcus aureus. Int. J. Antimicrob. Agents 46, 713–717. https://doi.org/10.1016/j.ijantimicag.2015.09.007.

Dikić, J., Lukić, I., Pajnik, J., Pavlović, J., Hrenović, J., Rajić, N., 2021. Antibacterial activity of thymol/carvacrol and clinoptilolite composites prepared by supercritical solvent impregnation. J. Porous Mater. 28, 1577–1584. https://doi.org/10.1007/s10934-021-01107-y.

Fernandes Costa, A., Evangelista Araujo, D., Santos Cabral, M., Teles Brito, I., de Menezes, B., Leite, L., Pereira, M., Correa Amaral, A., 2018. Development, characterization, and*in vitro–in vivo*evaluation of polymeric nanoparticles containing

miconazole and farnesol for treatment of vulvovaginal candidiasis. Med. Mycol. 57, 52–62. https://doi.org/10.1093/mmy/myx155.
Fernandes, R.A., Monteiro, D.R., Arias, L.S., Fernandes, G.L., Delbem, A.C.B., Barbosa, D. B., 2018. Virulence factors in *Candida albicans* and *Streptococcus mutans* biofilms mediated by farnesol. Indian J. Microbiol. 58, 138–145. https://doi.org/10.1007/s12088-018-0714-4.
Filoche, S.K., Soma, K., Sissons, C.H., 2005. Antimicrobial effects of essential oils in combination with chlorhexidine digluconate. Oral Microbiol. Immunol. 20, 221–225. https://doi.org/10.1111/j.1399-302x.2005.00216.x.
Gámez, E., Mendoza, G., Salido, S., Arruebo, M., Irusta, S., 2019. Antimicrobial Electrospun polycaprolactone-based wound dressings: an in vitro study about the importance of the direct contact to elicit bactericidal activity. Adv. Wound Care (new Rochelle) 8, 438–451. https://doi.org/10.1089/wound.2018.0893.
Gámez, E., Elizondo-Castillo, H., Tascon, J., García-Salinas, S., Navascues, N., Mendoza, G., Arruebo, M., Irusta, S., 2020. Antibacterial effect of thymol loaded SBA-15 nanorods incorporated in PCL electrospun fibers. Nanomaterials (basel) 10, 616. https://doi.org/10.3390/nano10040616.
Gámez-Herrera, E., García-Salinas, S., Salido, S., Sancho-Albero, M., Andreu, V., Pérez, M., Luján, L., Irusta, S., Arruebo, M., Mendoza, G., 2020. Drug-eluting wound dressings having sustained release of antimicrobial compounds. Eur. J. Pharm. Biopharm. 152, 327–339. https://doi.org/10.1016/j.ejpb.2020.05.025.
García-Salinas, S., Evangelopoulos, M., Gámez-Herrera, E., Arruebo, M., Irusta, S., Taraballi, F., Mendoza, G., Tasciotti, E., 2020a. Electrospun anti-inflammatory patch loaded with essential oils for wound healing. Int. J. Pharm. 577, 119067 https://doi.org/10.1016/j.ijpharm.2020.119067.
Garcia-Salinas, S., Gámez, E., Landa, G., Arruebo, M., Irusta, S., Mendoza, G., 2020. Antimicrobial wound dressings against fluorescent and methicillin-sensitive intracellular pathogenic bacteria. ACS Appl. Mater. Interfaces 12, 51302–51313. https://doi.org/10.1021/acsami.0c17043.
García-Salinas, S., Gámez, E., Asín, J., de Miguel, R., Andreu, V., Sancho-Albero, M., Mendoza, G., Irusta, S., Arruebo, M., 2020b. Efficiency of antimicrobial electrospun thymol-loaded polycaprolactone mats in vivo. ACS Appl. Bio Mater. 3, 3430–3439. https://doi.org/10.1021/acsabm.0c00419.
Gracia, R., Yus, C., Abian, O., Mendoza, G., Irusta, S., Sebastian, V., Andreu, V., Arruebo, M., 2018. Enzyme structure and function protection from gastrointestinal degradation using enteric coatings. Int. J. Biol. Macromol. 119, 413–422. https://doi.org/10.1016/j.ijbiomac.2018.07.143.
Hall, C.W., Mah, T.-F., 2017. Molecular mechanisms of biofilm-based antibiotic resistance and tolerance in pathogenic bacteria. FEMS Microbiol. Rev. 41, 276–301. https://doi.org/10.1093/femsre/fux010.
Huanbutta, K., Sittikijyothin, W., Sangnim, T., 2019. Development and characterization of bilayer wound healing patch nanofiber fabricated by electrospinning. J. Nano Res. 59, 46–56. https://doi.org/10.4028/www.scientific.net/jnanor.59.46.
Inoue, Y., Shiraishi, A., Hada, T., Hirose, K., Hamashima, H., Shimada, J., 2004. The antibacterial effects of terpene alcohols on Staphylococcus aureus and their mode of action. FEMS Microbiol. Lett. 237, 325–331. https://doi.org/10.1111/j.1574-6968.2004.tb09714.x.
Jabra-Rizk, M.A., Meiller, T.F., James, C.E., Shirtliff, M.E., 2006. Effect of farnesol on Staphylococcus aureus biofilm formation and antimicrobial susceptibility. Antimicrob. Agents Chemother. 50, 1463–1469. https://doi.org/10.1128/AAC.50.4.1463-1469.2006.
Jian, H.-J., Yu, J., Li, Y.-J., Unnikrishnan, B., Huang, Y.-F., Luo, L.-J., Hui-Kang Ma, D., Harroun, S.G., Chang, H.-T., Lin, H.-J., Lai, J.-Y., Huang, C.-C., 2020. Highly adhesive carbon quantum dots from biogenic amines for prevention of biofilm formation. Chem. Eng. J. 386, 123913 https://doi.org/10.1016/j.cej.2019.123913.
Jian, H.-J., Anand, A., Lai, J.-Y., Unnikrishnan, B., Chang, H.-T., Harroun, S.G., Huang, C.-C., 2023. In situ hybridization of polymeric curcumin to arginine-derived carbon quantum dots for synergistic treatment of bacterial infections. ACS Appl. Mater. Interfaces 15, 26457–26471. https://doi.org/10.1021/acsami.3c04316.
Kaneko, M., Togashi, N., Hamashima, H., Hirohara, M., Inoue, Y., 2011. Effect of farnesol on mevalonate pathway of Staphylococcus aureus. J. Antibiot. (Tokyo) 64, 547–549. https://doi.org/10.1038/ja.2011.49.
Karpanen, T.J., Worthington, T., Hendry, E.R., Conway, B.R., Lambert, P.A., 2008. Antimicrobial efficacy of chlorhexidine digluconate alone and in combination with eucalyptus oil, tea tree oil and thymol against planktonic and biofilm cultures of Staphylococcus epidermidis. J. Antimicrob. Chemother. 62, 1031–1036. https://doi.org/10.1093/jac/dkn325.
Koo, H., 2003. Inhibition of Streptococcus mutans biofilm accumulation and polysaccharide production by apigenin and tt-farnesol. J. Antimicrob. Chemother. 52, 782–789. https://doi.org/10.1093/jac/dkg449.
Krizanova, O., Penesova, A., Sokol, J., Hokynkova, A., Samadian, A., Babula, P., 2022. Signaling pathways in cutaneous wound healing. Front. Physiol. 13, 1030851. https://doi.org/10.3389/fphys.2022.1030851.
Li, Y.-J., Wei, S.-C., Chu, H.-W., Jian, H.-J., Anand, A., Nain, A., Huang, Y.-F., Chang, H.-T., Huang, C.-C., Lai, J.-Y., 2022. Poly-quercetin-based nanoVelcro as a multifunctional wound dressing for effective treatment of chronic wound infections. Chem. Eng. J. 437, 135315 https://doi.org/10.1016/j.cej.2022.135315.
Liu, X., Ma, X., Kun, E., Guo, X., Yu, Z., Zhang, F., 2018. Influence of lidocaine forms (salt vs. freebase) on properties of drug–eudragit® L100–55 extrudates prepared by reactive melt extrusion. Int. J. Pharm. 547, 291–302. https://doi.org/10.1016/j.ijpharm.2018.06.009.
Luo, L.-J., Nguyen, D.D., Huang, C.-C., Lai, J.-Y., 2022. Therapeutic hydrogel sheets programmed with multistage drug delivery for effective treatment of corneal abrasion. Chem. Eng. J. 429, 132409 https://doi.org/10.1016/j.cej.2021.132409.
Milovanovic, S., Markovic, D., Aksentijevic, K., Stojanovic, D.B., Ivanovic, J., Zizovic, I., 2016. Application of cellulose acetate for controlled release of thymol. Carbohydr. Polym. 147, 344–353. https://doi.org/10.1016/j.carbpol.2016.03.093.
Miranda-Calderon, L., Yus, C., Landa, G., Mendoza, G., Arruebo, M., Irusta, S., 2022. Pharmacokinetic control on the release of antimicrobial drugs from pH-responsive electrospun wound dressings. Int. J. Pharm. 624, 122003 https://doi.org/10.1016/j.ijpharm.2022.122003.
Mirhaj, M., Labbaf, S., Tavakoli, M., Seifalian, A., 2022. An Overview on the recent advances in the treatment of infected wounds: antibacterial wound dressings. Macromol. Biosci. 22, 2200014. https://doi.org/10.1002/mabi.202200014.
Nowacka, M., Kowalewska, A., Kręgiel, D., 2020. Farnesol-containing macromolecular systems for antibiofilm strategies. Surfaces 3, 197–210. https://doi.org/10.3390/surfaces3020015.
Oliveira, D., Borges, A., Saavedra, M.J., Borges, F., Simões, M., 2022. Screening of natural molecules as adjuvants to topical antibiotics to treat *Staphylococcus aureus* from diabetic foot ulcer infections. Antibiotics (basel) 11, 620. https://doi.org/10.3390/antibiotics11050620.
Parham, S., Kharazi, A.Z., Bakhsheshi-Rad, H.R., Kharaziha, M., Ismail, A.F., Sharif, S., Razzaghi, M., RamaKrishna, S., Berto, F., 2022. Antimicrobial synthetic and natural polymeric nanofibers as wound dressing: A review. Adv. Eng. Mater. 24, 2101460. https://doi.org/10.1002/adem.202101460.
Phillips, P.L., Yang, Q., Davis, S., Sampson, E.M., Azeke, J.I., Hamad, A., Schultz, G.S., 2015. Antimicrobial dressing efficacy against mature *Pseudomonas aeruginosa* biofilm on porcine skin explants. Int. Wound J. 12, 469–483. https://doi.org/10.1111/iwj.12142.
Pietsch, F., Heidrich, G., Nordholt, N., Schreiber, F., 2021. Prevalent synergy and antagonism among antibiotics and biocides in *Pseudomonas aeruginosa*. Front. Microbiol. 11, 615618 https://doi.org/10.3389/fmicb.2020.615618.
Ramamoorthy, M., Rajiv, S., 2015. In-vitro release of fragrant l-carvone from electrospun poly(ϵ-caprolactone)/wheat cellulose scaffold. Carbohydr. Polym. 133, 328–336. https://doi.org/10.1016/j.carbpol.2015.07.015.
Rueda-Fernández, M., Melguizo-Rodríguez, L., Costela-Ruiz, V.J., de Luna-Bertos, E., Ruiz, C., Ramos-Torrecillas, J., Illescas-Montes, R., 2022. Effect of the most common wound antiseptics on human skin fibroblasts. Clin. Exp. Dermatol. 47, 1543–1549. https://doi.org/10.1111/ced.15235.
Sato, T., Watanabe, T., Mikami, T., Matsumoto, T., 2004. Farnesol, a morphogenetic autoregulatory substance in the dimorphic fungus *Candida albicans*, inhibits hyphae growth through suppression of a mitogen-activated protein kinase cascade. Biol. Pharm. Bull. 27, 751–752. https://doi.org/10.1248/bpb.27.751.
Sousa, F.L., Horta, S., Santos, M., Rocha, S.M., Trindade, T., 2012. Release behavior of trans, trans-farnesol entrapped in amorphous silica capsules. Results Pharma Sci. 2, 52–56. https://doi.org/10.1016/j.rinphs.2012.07.001.
Sun, L., Ouyang, J., Zeng, F., Wu, S., 2022. An AIEgen-based oral-administration nanosystem for detection and therapy of ulcerative colitis via 3D-MSOT/NIR-II fluorescent imaging and inhibiting NLRP3 inflammasome. Biomaterials 283, 121468. https://doi.org/10.1016/j.biomaterials.2022.121468.
Togashi, N., Hamashima, H., Shiraishi, A., Inoue, Y., Takano, A., 2010. Antibacterial activities Against*Staphylococcus aureus*of terpene alcohols with aliphatic carbon chains. J. Essent. Oil Res. 22, 263–269. https://doi.org/10.1080/10412905.2010.9700321.
Turanlı, Y., Acartürk, F., 2021. Fabrication and characterization of budesonide loaded colon-specific nanofiber drug delivery systems using anionic and cationic polymethacrylate polymers. J. Drug Deliv. Sci. Technol. 63, 102511 https://doi.org/10.1016/j.jddst.2021.102511.
Ullah, A., Jang, M., Khan, H., Choi, H.J., An, S., Kim, D., Kim, Y.-R., Kim, U.-K., Kim, G. M., 2021. Microneedle array with a pH-responsive polymer coating and its application in smart drug delivery for wound healing. Sens. Actuators B Chem. 345, 130441 https://doi.org/10.1016/j.snb.2021.130441.
Valcourt, C., Buyck, J.M., Grégoire, N., Couet, W., Marchand, S., Tewes, F., 2021. Lipid nanoparticles loaded with farnesol or geraniol to enhance the susceptibility of *E. coli* MCR-1 to Colistin. Pharmaceutics 13, 1849. https://doi.org/10.3390/pharmaceutics13111849.
Wei, M., Jiang, Q., Niu, N., Dong, L., Wang, L., Chen, W., Fu, Q., Chen, Y., Wang, J., 2019. Reduction of biofilm in chronic wounds by antibacterial protease combined with silver dressing. Int J Clin Exp Med 12 (10), 12293–12302. Retrieved from. https://e-century.us/files/ijcem/12/10/ijcem0096924.pdf.
Wu, G.-X., Wang, Y.-W., Wu, C.-S., Lin, Y.-H., Hung, C.-H., Huang, H.-H., Kuo, S.-M., 2021. Therapeutic efficacy of sesquiterpene farnesol in treatment of Cutibacterium acnes-induced dermal disorders. Molecules 26, 5723. https://doi.org/10.3390/molecules26185723.
Wu, Y.C., Wu, G.X., Huang, H.H., Kuo, S.M., 2019. Liposome-encapsulated farnesol accelerated tissue repair in third-degree burns on a rat model. Burns 45, 1139–1151. https://doi.org/10.1016/j.burns.2019.01.010.
Yang, C., Nguyen, D.D., Lai, J., 2023. Poly(l-Histidine)-mediated on-demand therapeutic delivery of roughened ceria nanocages for treatment of chemical eye injury. Adv. Sci. 10 https://doi.org/10.1002/advs.202302174.
Yenice Gürsu, B., 2020. Potential antibiofilm activity of farnesol-loaded poly(DL-lactide-co-glycolide) (PLGA) nanoparticles against *Candida albicans*. J. Anal. Sci. Technol. 11 https://doi.org/10.1186/s40543-020-00241-7.
Zamani, M., Prabhakaran, M.P., Ramakrishna, S., 2013. Advances in drug delivery via electrospun and electrosprayed nanomaterials. Int. J. Nanomed. 8, 2997–3017. https://doi.org/10.2147/IJN.S43575.
Zheng, X., Chen, L., Zeng, W., Liao, W., Wang, Z., Tian, X., Fang, R., Sun, Y., Zhou, T., 2021. Antibacterial and anti-biofilm efficacy of Chinese dragon's blood against *Staphylococcus aureus* isolated from infected wounds. Front. Microbiol. 12, 672943 https://doi.org/10.3389/fmicb.2021.672943.